nature communications

Article

https://doi.org/10.1038/s41467-025-62342-4

An RNA modification prevents extended codon-anticodon interactions from facilitating +1 frameshifting

Received: 22 September 2024

Accepted: 19 July 2025

Published online: 11 August 2025

Check for updates

Evelyn M. Kimbrough[1], Ha An Nguyen[1], Haixing Li[2,5], Jacob M. Mattingly[1,3], Nevette A. Bailey[2], Wei Ning[2], Howard Gamper[4], Ya-Ming Hou[4], Ruben L. Gonzalez Jr.[2] ✉ & Christine M. Dunham[1] ✉

RNA post-transcriptional modifications act by stabilizing the functional conformations of RNA. While their role in messenger RNA (mRNA) decoding is well established, it is less clear how transfer RNA (tRNA) modifications outside the anticodon contribute to tRNA stability and accurate protein synthesis. Absence of such modifications causes translation errors, including mRNA frameshifting. By integrating single-molecule fluorescence resonance energy transfer and cryogenic electron microscopy, we demonstrate that the N^1-methylguanosine (m^1G) modification at position 37 of *Escherichia coli* $tRNA^{ProL}$ is necessary and sufficient for modulating the conformational energy of this tRNA on the ribosome so as to suppress +1 frameshifting otherwise induced by this tRNA. Six structures of *E. coli* ribosomal complexes carrying $tRNA^{ProL}$ lacking m^1G37 show this tRNA forms four and even five codon-anticodon base pairs as it moves into the +1 frame, allowing direct visualization of the long-standing hypothesis that a four base pair codon-anticodon can form during +1 frameshifting.

The ribosome decodes three-nucleotide codons in messenger RNA (mRNA) to sequentially add amino acids to the nascent polypeptide chain. In specific circumstances, the ribosome can deviate from the triplet code and "frameshift" in either the forward (+) or backward (-) direction on mRNA. This change in the mRNA reading frame produces a protein with a different amino acid sequence relative to the sequence defined by the original reading frame. Unintentional frameshifting can be caused by the loss of transfer RNA (tRNA) modifications[1–4], the low availability of aminoacyl (aa)-tRNAs[5], or ribosome collisions[6]. Such unintentional frameshifting can result in the accumulation of erroneous and toxic proteins that are detrimental to cellular function and, when unresolved, can hinder growth and cause cell death[7,8]. Frameshifting may also be intentional (programmed) and beneficial for the expression of multiple proteins from the same mRNA[9–11] and can be regulated by specific mRNA sequences, mRNA tertiary structures[12,13], or aa-tRNA levels[11,14–19].

The loss of tRNA modifications can lead to increases in the levels of frameshifting[1–4]. Such modifications normally provide structural integrity for tRNAs that are critical for translational accuracy and interactions with translation factors[20,21]. Although modified nucleotides are located extensively throughout the tRNA, the anticodon stem-loop is the most heavily modified region, with ~70% of all modifications occurring there[22]. tRNA modifications at the anticodon expand the ability to read the genetic code, with modifications at nucleotide 34 permitting non-Watson-Crick interactions with an mRNA nucleotide that resemble the geometry of Watson-Crick base pairs and are therefore accepted during decoding[20,22–24] (anticodon nucleotides are numbered 34, 35, 36) (Fig. 1a). On the 3' side of the anticodon, nucleotide 37 is also commonly modified, with this modification contributing its stacking with the anticodon during decoding, thereby preventing frameshifting and maintaining the reading frame[20,22–27]. One of the simplest modifications at nucleotide 37 is a

[1]Department of Chemistry, Emory University, Atlanta, GA, USA. [2]Department of Chemistry, Columbia University, New York, NY, USA. [3]Graduate Program in Biochemistry, Cell and Developmental Biology, Emory University, Atlanta, GA, USA. [4]Department of Biochemistry and Molecular Biology, Thomas Jefferson University, Philadelphia, PA, USA. [5]Present address: Department of Physics, City University of Hong Kong, Kowloon, Hong Kong, China.
✉e-mail: rlg2118@columbia.edu; christine.m.dunham@emory.edu

https://doi.org/10.1038/s41467-025-62342-4

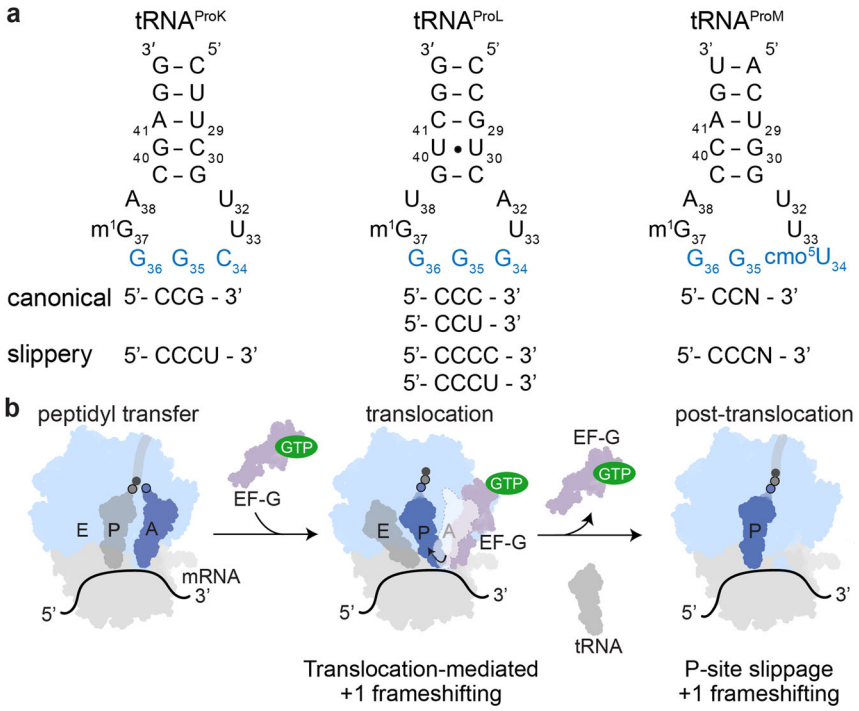

Fig. 1 | Mechanisms of +1 frameshifting by tRNA^{Pro} isoacceptors. a The anticodon stem-loop (ASL; 18 nucleotides) of tRNA^{Pro} isoacceptors and their corresponding anticodons (blue), including the four nucleotide codons that induce +1 frameshifting in the absence of m^{1}G37. cmo^5 denotes a 5-oxyacetic acid uridine modification. N denotes any A/U/G/C nucleotide. **b** The absence of m^{1}G37 in tRNA^{ProL} induces a +1 frameshift on proline slippery codons at two defined substeps during the elongation cycle: during the EF-G-mediated translocation of peptidyl-tRNA^{Pro} isoacceptor from the A site to the P site (middle) and after translocation, when the peptidyl-tRNA^{Pro} isoacceptor is positioned in the P site but the next A-site aa-tRNA hasn't been delivered yet (right).

single methyl group appended to guanosine at position N^1 (m^{1}G37). This modification is found in tRNA^{Pro}, tRNA^{Leu}, and tRNA^{Arg} isoacceptors and, in bacteria, is installed by the *S*-adenosyl-L-methionine (SAM)-dependent methyltransferase TrmD[1–3,28,29]. Deletion of TrmD is lethal, and reduction of TrmD levels leads to growth defects, slower translation rates, and an increase in +1 frameshifting, primarily at proline codons and, to a lesser extent, at arginine and leucine codons[1,2,7,8,30]. Additionally, a lack of m^{1}G37 in the tRNA^{ArgX} (CCG anticodon) isoacceptor and the tRNA^{ProL} (GGG anticodon), tRNA^{ProK} (CGG anticodon), and tRNA^{ProM} (UGG anticodon) isoacceptors results in inefficient aminoacylation of these tRNAs, preventing them from entering the translation cycle and causing growth arrest[7,31,32].

While several tRNAs contain m^{1}G37, this modification is particularly important for suppressing unintentional frameshifting in the tRNA^{Pro} family of isoacceptors[3,7,30,33]. Lack of m^{1}G37 in these three tRNAs induces +1 frameshifting at "slippery" codons that usually consist of a stretch of repetitive nucleotides (Fig. 1a)[3]. The tRNA^{Pro} isoacceptors can induce +1 frameshifting at slippery codons during either or both of two substeps of the ribosomal elongation cycle[3,4,34]. The first substep is the Elongation Factor (EF) G-mediated translocation of peptidyl-tRNA^{Pro} from the ribosomal aa-tRNA binding (A) site to the ribosomal peptidyl-tRNA binding (P) site. The second is after translocation, when the peptidyl-tRNA^{Pro} isoacceptor is positioned in the P site but before delivery of the next A-site aa-tRNA (Fig. 1b). For the tRNA^{Pro} isoacceptors, the absence of m^{1}G37 increases +1 frameshifting to varying extents in each of the isoacceptors[3,30,33]. This variation indicates that other nucleotides and/or modifications specific to each isoacceptor and/or the 'slipperiness' of the codon may also contribute to reading frame maintenance and/or frameshifting. Moreover, it suggests that the mechanism(s) through which m^{1}G37 contributes to frameshift suppression by each tRNA^{Pro} isoacceptor may be distinct. Consistent with this, tRNA^{ProM} lacking m^{1}G37 is likelier to frameshift during translocation than a tRNA^{ProL} lacking m^{1}G37, whereas, in the absence of m^{1}G37, both tRNAs are prone to frameshift in the P site[3,35]. Similarly, whereas m^{1}G37 is the single determinant that suppresses frameshifting by tRNA^{ProM}, both m^{1}G37 and EF-P contribute to maximizing suppression of frameshifting by tRNA^{ProL}[3]. In other words, suppression of +1 frameshifting by tRNA^{ProL} at a CCC-C slippery codon does not require both m^{1}G37 and EF-P, and it is only enhanced by the action of both. Furthermore, over-expression of tRNA^{ProM} increases frameshifting rates, while over-expression of tRNA^{ProL} reduces frameshifting rates[33].

In this study, we used single-molecule fluorescence resonance energy transfer (smFRET) imaging and cryogenic electron microscopy (cryo-EM) to extend our understanding of how m^{1}G37 in tRNA^{ProL} contributes to reading frame maintenance in the presence of slippery codons. We focused on tRNA^{ProL} because m^{1}G37 is the only modification in the anticodon loop of this isoacceptor that directly contributes to reading frame maintenance[36] (whereas tRNA^{ProM} carries m^{1}G37 as well as a 5-carboxymethoxyuridine at nucleotide 34 (cmo^{5}U34), both of which influence +1 frameshifting). Our smFRET results reveal that the m^{1}G37 modification is both necessary and sufficient for modulating the conformational energy of a fully unmodified, P site-bound tRNA^{ProL} that would otherwise induce frameshifting when this tRNA it is paired to a slippery codon. This observation strongly suggests that at least part of the mechanism through which m^{1}G37 suppresses +1 frameshifting is by stabilizing conformations of the P site-bound, slippery codon-paired tRNA^{ProL} that resist frameshifting. Consistent with this, cryo-EM structures of similar ribosomal complexes show that the absence of m^{1}G37 in a P site-bound, slippery codon-paired tRNA^{ProL} enables this tRNA to adopt a wide range of ribosome-bound conformations, some of which permit four and even five codon-anticodon base pairs to form. This is notable, as it is the first time more than three codon-anticodon base pairs have been observed on the ribosome, despite the possibility of this having been raised over four decades ago[37–40]. Delivery of an A-site tRNA in the +1 frame to these ribosomal complexes stabilizes tRNA^{ProL} and reestablishes interactions with the P site of the ribosome with translation

proceeding in the +1 frame. Collectively, these data provide important insights into the influence that m^{1}G37 has on the conformational energetics of P site-bound tRNA^{ProL} and how modulation of these energetics stabilizes tRNA conformations within the P site that maintain the reading frame.

Results

m^{1}G37 stabilizes a conformation of the P site-bound, slippery codon-paired tRNA^{ProL} that suppresses frameshifting

Two types of ribosomal complexes were used in the studies reported here. The first type is post-translocation complexes carrying a tRNA^{ProL} isoacceptor in the P site that is aminoacylated to mimic peptidylation (hereafter referred to as "POST"). The second type is analogous to POST with the exception that the P-site tRNA^{ProL} is deacylated to mimic a situation after peptidyl transfer (referred to as "POST−", where the "−" sign denotes the absence of an acylated group on the P-site tRNA). In previous smFRET studies, we have demonstrated that site-specific substitution mutations of the P-site tRNA can modulate the energetic stability of POST− complexes[41]. We hypothesized that m^{1}G37 of the P site-bound tRNA^{ProL} might have similar energetic effects. Such effects might specifically manifest only within the context of a slippery codon, thus regulating reading frame maintenance. To explore these possibilities, we used *Escherichia coli* translation components to perform smFRET experiments on a series of *E. coli* 70S POST− complexes of tRNA^{ProL} with or without the m^{1}G37 at the proline CCC-C slippery codon or the proline CCC-G non-slippery codon at the P site (Fig. 2). These complexes were formed using ribosomal large, or 50S, subunits in which ribosomal proteins bL9 and uL1 ribosomal proteins have been labeled with the

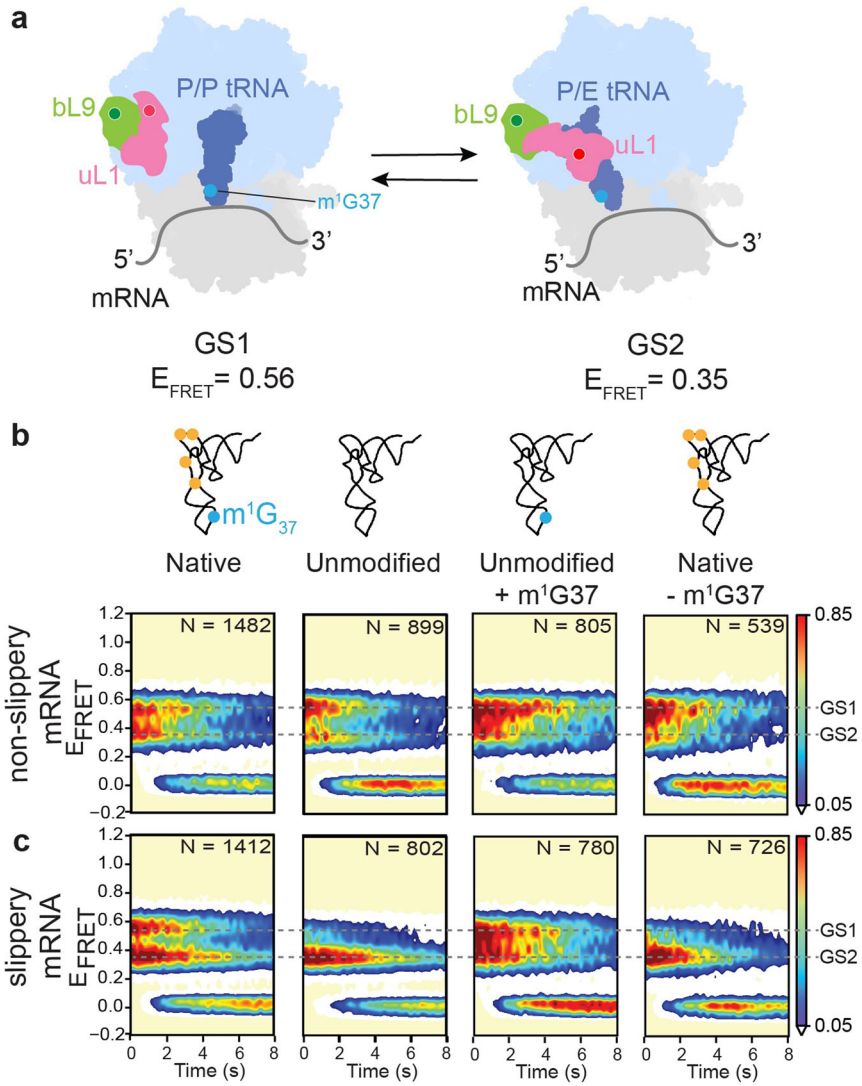

Fig. 2 | Influence of G37 modification status and codon slipperiness on P-site tRNA^{ProL} conformational energy. a Cartoon of the GS1⇄GS2 conformational equilibrium of a POST− complex containing Cy3- and Cy5-labeled ribosomal proteins bL9 and uL1, respectively, and carrying a P site-bound tRNA^{ProL}. Among other structural differences, GS1 features a P/P-configured tRNA and an open uL1 stalk, resulting in an E_{FRET} value of 0.55. In contrast, GS2 features a P/E-configured tRNA and a closed uL1 stalk, resulting in an E_{FRET} value of 0.35. **b**, **c** Surface contour plots are generated by superimposing numerous individual E_{FRET} *vs.* time trajectories (Supplemental Fig. S1) recorded using smFRET experiments conducted on eight POST− complexes. Contours are colored from white (lowest population) to red (highest population), as indicated, and N at the rightmost top of each surface contour plot specifies the number of E_{FRET} trajectories that were used to construct that plot. The eight POST− complexes carried either P-site native, unmodified, unmodified +m^{1}G37, or native −m^{1}G37 variants of tRNA^{ProL}, as specified by the tRNA cartoons along the top of the four columns of surface contour plots. In these cartoons, m^{1}G37 is indicated in blue, and other tRNA^{ProL} modifications are depicted in yellow. In addition, these POST− complexes were formed using mRNAs that place either a proline CCC-G non-slippery codon or a proline CCC-C slippery codon at the P site, as specified along the left of the two rows of surface contour plots. A detailed description of how the smFRET data were analyzed, including how the % GS1, % GS2, K_{eq}, $k_{GS1\to GS2}$, and $k_{GS2\to GS1}$ were calculated, can be found in the "Materials and Methods".

FRET donor Cy3 and the FRET Cy5 acceptor, respectively, generating a bL9-uL1 smFRET signal[42,43] (Note: "b" refers to a bacterial-only ribosomal protein and "u" refers to a universal ribosomal protein[44]) (Fig. 2a). Previously, we showed that the bL9-uL1 smFRET signal within POST− complexes fluctuates between two FRET states, corresponding to Global State 1 (GS1, E_{FRET}s of ~0.56) and Global State 2 (GS2, E_{FRET}s of ~0.35), and reports on a GS1⇄GS2 conformational equilibrium[43]. We use smFRET to quantitatively characterize this equilibrium by measuring the rates of transitions (*k*s) between GS1 and GS2 ($k_{GS1\rightarrow GS2}$ and $k_{GS2\rightarrow GS1}$) and the corresponding equilibrium constant ($K_{eq} = k_{GS1\rightarrow GS2}/k_{GS2\rightarrow GS1}$)[43] (Fig. S1).

Among other structural differences, GS1 and GS2 feature P-site tRNAs that occupy the classical "P/P" or the hybrid "P/E" configurations, respectively. The P/P notation specifies that the P-site tRNA occupies the P sites of both the ribosomal small, or 30S, subunit and the 50S subunit, whereas the P/E notation specifies that the P-site tRNA occupies the P site of the 30S subunit and the ribosomal tRNA exit (E) site of the 50S subunit. Consequently, all other things being equal, the GS1⇄GS2 equilibrium of a particular POST− complex reports on the relative stabilities of the P/P and P/E configurations of the P-site tRNA, stabilities we expect to depend on the conformational energetics of the tRNA and the tRNA-codon complex within the P site. Consistent with this, our previous work showed that changes in the acylation state[43], acylation identity[41,43], and individual nucleotides[41] of the P-site tRNA can alter the relative stabilities of the P/P and P/E configurations in a POST−complex. Here, we performed bL9-uL1 smFRET experiments on a series of POST− complexes carrying P-site $tRNA^{ProL}$. By varying the modification status of $tRNA^{ProL}$ and the slippery or non-slippery context of the proline codon it interacts with, we have investigated whether and how these features modulate the relative stabilities of the P/P and P/E configurations of the P-site tRNA within the POST− complexes (Fig. 2b, c and Table S1).

We began by investigating POST− complexes carrying P-site $tRNA^{ProL}$ in the "native" state (i.e., containing all of its natural modifications) or the "unmodified" state (i.e., lacking any modifications) at the slippery codon. Our results reveal that native $tRNA^{ProL}$ is thermodynamically stabilized in the P/P configuration by 2.2-fold over unmodified $tRNA^{ProL}$ (i.e., the K_{eq} of native $tRNA^{ProL}$ is 2.2-fold lower than that of unmodified $tRNA^{ProL}$). Kinetically, this is driven by a small, 13% decrease in $k_{GS1\rightarrow GS2}$ and a larger, 2.2-fold increase in $k_{GS2\rightarrow GS1}$ for native $tRNA^{ProL}$ relative to unmodified $tRNA^{ProL}$ (Fig. 2b, c and Table S1). This finding strongly suggests that at a slippery codon, native $tRNA^{ProL}$ adopts a conformation, or set of conformations, that is different relative to unmodified $tRNA^{ProL}$. This conformational difference, whatever its nature, arises from a small stabilization of the P/P configuration that underlies the 13% decrease in $k_{GS1\rightarrow GS2}$ and a large destabilization of the P/E configuration that underlies the 2.2-fold increase in $k_{GS2\rightarrow GS1}$ for the native $tRNA^{ProL}$ relative to the unmodified $tRNA^{ProL}$.

Analyses of the remaining POST− complexes show that the conformational difference between the native and unmodified $tRNA^{ProL}$ at a slippery codon is fully dependent on and solely realized by m^1G37 and that such a conformational difference is not detected at a non-slippery codon (Fig. 2b, c). Specifically, a POST− complex carrying a P-site $tRNA^{ProL}$ in the "unmodified +m^1G37" state (i.e., containing only the m^1 modification at G37) at the slippery codon exhibits a K_{eq} and *k*s that closely resemble those of the POST− complex carrying a P-site native $tRNA^{ProL}$, only differing by an average of 28%. Consistent with what we observed for the native $tRNA^{ProL}$, the unmodified +m^1G37 $tRNA^{ProL}$ at the slippery codon is thermodynamically stabilized in the P/P configuration by 2.8-fold over the unmodified $tRNA^{ProL}$ and 1.9-fold over a POST− complex carrying a P-site $tRNA^{ProL}$ in the "native −m^1G37" state (i.e., lacking only the m^1 modification at G37), respectively. Moreover, likewise consistent with what we observed for native $tRNA^{ProL}$, these increases in thermodynamic stabilities are kinetically driven by small, 35% and 27%, decreases in $k_{GS1\rightarrow GS2}$ and larger, 3.3- and 2.3-fold, increases in $k_{GS2\rightarrow GS1}$ for unmodified +m^1G37 $tRNA^{ProL}$ relative to unmodified and native −m^1G37 $tRNA^{ProL}$, respectively.

Demonstrating that these m^1G37-dependent energetic differences are only detected at a slippery codon, we find that the K_{eq}s and *k*s of $tRNA^{ProL}$ species formed at a non-slippery codon vary by only an average of 41% across all POST− complexes formed at a non-slippery codon, regardless of the modification status of G37. Collectively, these results strongly suggest that the m^1 modification at G37 is both necessary and sufficient to allow native $tRNA^{ProL}$ to adopt a conformation, or set of conformations, at a slippery codon that differs significantly from that which it adopts in the absence of the m^1G37 modification. The fact that this conformational difference is not observed at a non-slippery codon presents the possibility that the m^1G37-dependent conformation(s) of the native $tRNA^{ProL}$ we identify here contributes to the mechanism through which the m^1 modification at G37 suppresses +1 frameshifting at slippery codons. These data, which were recorded using POST− complexes lacking an A-site tRNA, are also consistent with prior biochemical data demonstrating that a slippery codon-paired $tRNA^{ProL}$ can frameshift in the P site prior to the delivery of an A-site tRNA[3]. In the sections below, we report structural studies aimed at investigating this possibility.

Cryo-EM structures of POST− complexes carrying an unmodified $tRNA^{ProL}$ in the P site

To visualize how the lack of m^1G37 alters the conformation and position of $tRNA^{ProL}$ in POST− complexes, as identified in the smFRET data, we determined a cryo-EM structure of a deacylated unmodified $tRNA^{ProL}$ paired to the CCC-C slippery codon in the P site of a POST− complex (Fig. 3; Table S2, and Figs. S2, S3). The dataset captured six populations, with the majority (~41%) of particles showing unmodified

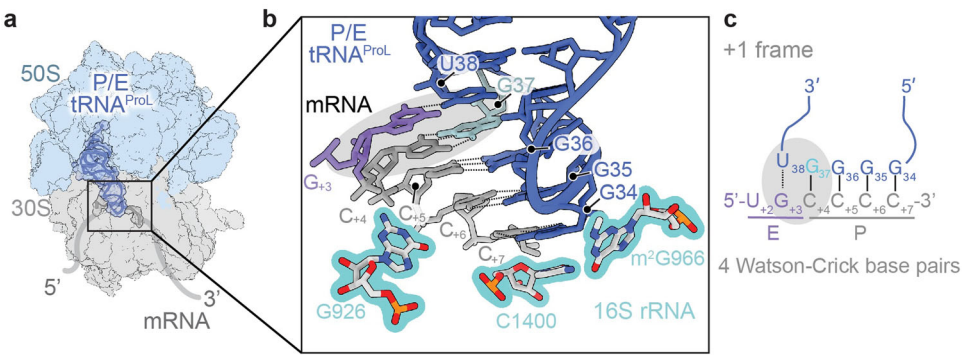

Fig. 3 | Four Watson-Crick base pairs form during +1 frameshifting of $tRNA^{ProL}$. **a** A 2.9 Å cryo-EM structure of a ribosomal POST− complex carrying a P/E-configured, unmodified $tRNA^{ProL}$ at a CCC-C slippery codon in the +1 frame. **b** Close-up of the codon-anticodon reveals four Watson-Crick base pairs and an interaction between U38 in the anticodon stem-loop and G_{+3} in the codon. The additional base pairs are highlighted in gray (and in **c**). **c** A schematic of these interactions.

tRNA^{ProL} adopting a P/E configuration (Fig. S2). One other population, which is discussed below, showed two tRNAs bound in the P and the A sites. The other four populations suffer from low resolution of both the tRNA and the codon-anticodon interactions, preventing us from identifying the tRNA species and building the codon-anticodon complex, despite the high resolution (2.9 Å–3.8 Å) of the overall structures (Fig. S2).

The structure containing unmodified P/E-configured tRNA^{ProL} has an overall resolution of 2.9 Å, with a high enough quality of the map surrounding the codon-anticodon interaction such that we can unequivocally model the interaction. Specifically, unmodified tRNA^{ProL} adopts the P/E configuration within the POST– complex, consistent with the preferential configuration we observed P-site bound, unmodified tRNA^{ProL} to adopt at a slippery codon in our smFRET experiments of the analogous POST– complex (Fig. 2b). The movement of tRNA^{ProL} into the P/E configuration also causes a slight ~4.2° rotation of the 30S 'head' domain, similar to the rotation observed in other ribosomal complexes carrying P/E-configured tRNAs[45]. The movement of tRNA^{ProL} lacking m^{1}G37 from the P/P to the P/E configuration is also consistent with the structures of ribosomal complexes undergoing frameshifting induced by tRNA^{ProK} lacking m^{1}G37[27]. Surprisingly, four Watson-Crick base pairs are visualized between the anticodon (G37, G36, G35, and G34 nucleotides) and the slippery codon (C_{+4}, C_{+5}, C_{+6}, and C_{+7} nucleotides), respectively, with an additional hydrogen bond forming between G_{+3} of the mRNA and U38 of the anticodon stem-loop (Fig. 3 and Fig. S4a). Four and five-base pair interactions between the codon and the anticodon have been predicted from prior genetic studies of frameshifting[37,38,40,46], but to our knowledge, this is the first time such interactions have been structurally captured. These results provide evidence for the importance of the m^{1}G37 modification on the energetics of the tRNA^{ProL}. Since tRNA^{ProL} would normally carry an aminoacyl group in the P site, which positions the tRNA predominantly in the P site, these data report on only the energetics of tRNA^{ProL} and its reliance on m^{1}G37.

When prevented from adopting the P/E configuration within a POST complex, P-site bound tRNA^{ProL} pairs with the slippery codon in the normal and +1 frames

Previous kinetic studies demonstrated that peptidyl-tRNA^{ProL} predominantly frameshifts in the P site prior to transfer of the peptide chain onto the amino acid of the incoming A-site aa-tRNA[3]. To structurally visualize this POST complex, we needed to prevent hydrolysis of the linkage between the aminoacyl group and our aa-tRNA^{ProL}. Using a flexizyme[47], we therefore aminoacylated lysine onto tRNA^{ProL} via a nonhydrolyzable linkage[48]. Lysine was used because the Lys-tRNA^{ProL} product was readily separated from the tRNA^{ProL} substrate on a denaturing electrophoresis gel, whereas Pro-tRNA^{ProL} could not be separated from its substrate tRNA^{ProL}. We then determined a cryo-EM structure of the POST complex containing an unmodified Lys-tRNA^{ProL} paired with a CCC-C slippery codon in the P site (Fig. 4; Fig. S5, Table S3). The dataset captured four populations: the majority (~ 60%) population, which was spread over two classes of particles, contains an unmodified Lys-tRNA^{ProL} in a P/P configuration, while in the two smaller populations, deacylated tRNA^{ProL} adopts the P/E configuration or a configuration between P/E and E/E (Fig. S5).

In the first class of particles carrying a P site-bound, unmodified Lys-tRNA^{ProL}, accounting for 32% of the total particles, the structure was determined to have an overall resolution of 3.5 Å (Fig. 4a, b and Fig. S6a, b). The tRNA adopts a P/P configuration and interacts with the slippery codon in the normal reading frame. In this case, tRNA^{ProL} forms three Watson-Crick base pairing interactions between anticodon nucleotides G36, G35, and G34 and codon nucleotides C_{+4}, C_{+5}, and C_{+6}, respectively (Figs. 4b and S7a). The second class contains ~28% of the particles

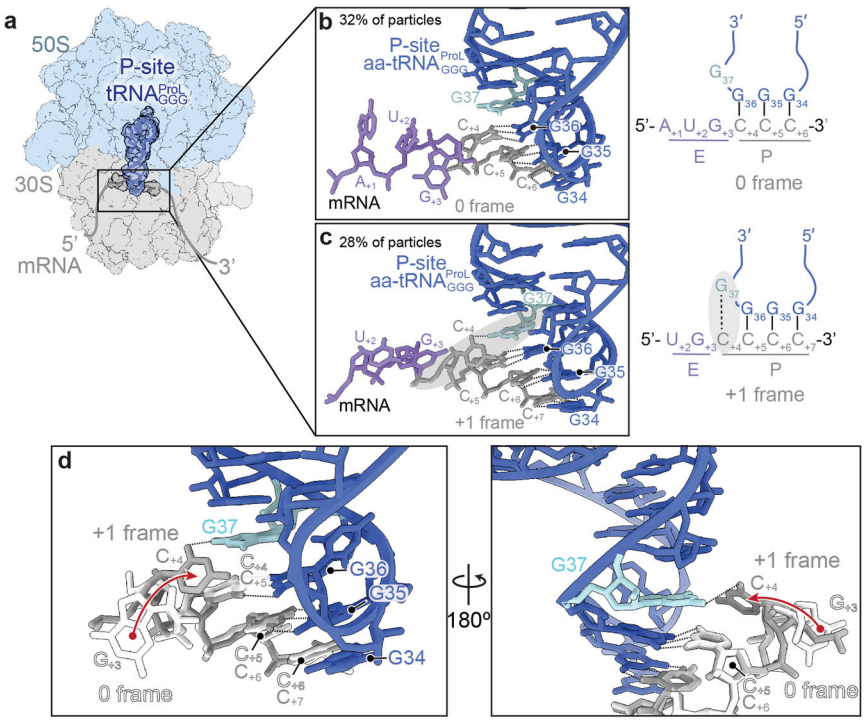

Fig. 4 | P site-bound, unmodified aa-tRNA^{ProL} can occupy the normal or +1 frames. a 3.5 Å (normal frame) and 3.6 Å (+1 frame) cryo-EM structures of POST complexes carrying an unmodified Lys-tRNA^{ProL} bound to a CCC-C slippery codon in the P site. **b** ~32% of particles show that the P-site tRNA^{ProL} interacts with the slippery codon in the normal frame, with formation of the three expected Watson-Crick base pairs (left). A schematic of these interactions is shown (right). **c** ~28% of particles show that the P-site Lys-tRNA^{ProL} interacts with the slippery codon in the +1 frame, with formation of three Watson-Crick base pairs and movement of the C_{+4} codon nucleotide moving towards G37 of the Lys-tRNA^{ProL}. The additional base pairs are highlighted in gray. A schematic of these interactions is shown (right). **d** One major difference in the codon-anticodon interaction between POST complexes in the normal or +1 frames is the way the mRNA interacts with the unmodified G37. In the normal frame, G_{+3} is positioned away from G37, whereas in the +1 frame C_{+4} flips towards G37.

and is resolved to an overall resolution of 3.6 Å, where the unmodified Lys-tRNA^{ProL} again adopts a P/P configuration (Fig. 4c and Fig. S6b). Contrasting with the first class of particles, however, tRNA^{ProL} in the second class of particles is in the +1 reading frame. Specifically, tRNA^{ProL} forms three Watson-Crick base pairing interactions, but the interactions are shifted by one nucleotide towards the 3′ end of the mRNA: these base pairs include G34-C$_{+7}$, G35-C$_{+6}$, and G36-C$_{+5}$ (Figs. 4c and S7b). In the +1 frame, the first nucleotide of the proline codon, nucleotide C$_{+4}$, is not positioned within the mRNA path of the E site but instead extends towards the anticodon loop of the P-site tRNA, within hydrogen bonding distance of the unmodified G37 (Fig. 4d). When G37 contains the m^1 modification, the hydrophobic methyl group is likely to sterically prevent interactions with the codon and thus help to preserve the codon-anticodon interaction in the normal frame. These structures demonstrate the importance of the m^1 modification at G37 in tRNA^{ProL} in maintaining the normal frame, consistent with functional studies showing that unmodified tRNA^{Pro} isoacceptors are prone to +1 frameshifting in the P site[3,34,35].

The mRNA located in the E site adopts a different conformation depending upon whether the codon-anticodon complex is in the normal or the +1 frame (Figs. 4b–d and S7). In the normal frame, G$_{+3}$ rotates towards 16S rRNA nucleotide G926, a nucleotide that is known to stabilize the mRNA position within the ribosome by forming a hydrogen bonding interaction with the phosphate backbone of the mRNA between the E- and P-site codons[49]. In the +1 frame, in which C$_{+4}$ moves towards G37 of the P-site tRNA, G$_{+3}$ is within the mRNA path in the E site and π-stacks with 16S rRNA nucleotide G693 and mRNA nucleotides U$_{+2}$ and C$_{+4}$ (Fig. S7b). This new position allows G926 to hydrogen bond with the phosphate backbones of C$_{+4}$ and U$_{+2}$ (Fig. S7b). Additionally, in the +1 frame, 16S rRNA nucleotide G693 is now π-stacked with U$_{+2}$ instead of A$_{+1}$.

The remaining two populations of particles show that tRNA^{ProL} occupies the P/E configuration or a configuration between P/E and E/E (Fig. S6c, S6d, S8 and Table S4). Because the flexizyme acylation is not 100% efficient at aminoacylating lysine onto tRNA^{ProL}, these two populations likely contain deacylated tRNA^{ProL}, which has a high affinity for the 50S E site while peptidyl-tRNAs (or aa-tRNAs) cannot bind to the 50S E site due to steric clashes with nucleotides C2394 and C2395 of the 23S rRNA component of the 50S subunit[50,51] (Fig. S9). One population, comprised of ~16% of the particles, shows tRNA^{ProL} in the P/E configuration at a resolution of ~4.0 Å (Figs. S5, S6c, S8) and the other population, comprised of ~24% of the particles, shows tRNA^{ProL} in a configuration between P/E and E/E that has previously been referred to as an e*/E configuration at a resolution of ~3.8 Å[27] (Figs. S5, S6d). In the 30S e* site, the tRNA is closer to the E site than the P site, similar to the tRNA position in structures of EF-G-bound ribosomal complexes captured in intermediate states of translocation and in ribosome structures of tRNAs that induce frameshifting[27,52–55]. Concomitant with the movement of tRNA^{ProL} towards the E site on the 30S subunit, the head domain of the 30S subunit swivels counterclockwise ~19.5° and tilts ~3.4°, a movement that has previously been seen in EF-G-bound ribosomal complexes[52,53]. The map quality for the anticodon stem-loop of tRNA^{ProL} in these two populations is low, indicating that this region is highly dynamic, preventing us from confidently modeling the codon-anticodon interaction.

Collectively, these structural results reveal that in the context of a P site-bound, unmodified tRNA^{Pro} at a slippery codon, the smFRET-observed GS1 state is likely comprised of multiple states in which the tRNA occupies the P/P configuration in either the normal or the +1 frame. We say "likely" here because whereas the smFRET experiments used a POST– complex carrying a deacylated tRNA^{ProL} at the P site, the ribosomal complexes for the cryo-EM studies were of a POST complex carrying an acylated Lys-tRNA^{ProL} at the P site. Thus, although unlikely, there could formally be some difference between the P/P configurations in the two complexes. Likewise, the GS2 state is comprised of multiple states in which the tRNA can occupy either the P/E or the e*/E configuration at either the normal or the +1 frame (the dynamics of the anticodon stem-loop and resulting map quality do not allow us to distinguish the frame). These structures reveal the structural basis for how the m^{1}G37 modification regulates the conformational energy of P site-bound tRNA^{ProL} so as to suppress +1 frameshifting on slippery codons. These results also demonstrate that the smFRET-observed GS1 and GS2 states in these complexes are comprised of multiple states and reveal the structural identities of these states at near-atomic resolution. Specifically, we show that the GS1 state is comprised of P/P-configured, unmodified tRNA^{ProL}s that occupy either the normal or the +1 frame, while the GS2 state is comprised of either P/E- or e*/E-configured, unmodified tRNA^{ProL}s in the normal or +1 frames.

Addition of A-site tRNA reinforces protein synthesis in the +1 frame

Previous kinetic studies showed that a tRNA^{ProL} lacking m^{1}G37 frameshifts in the P site prior to delivery of an A-site tRNA[3]. To understand the influence of an adjacent A-site tRNA on P site-bound, slippery codon-paired, unmodified tRNA^{ProL}, we determined the structure of this POST– complex. Sorting of the dataset yielded one major population (~20%) of particles containing both a P-site unmodified tRNA^{ProL} and an A-site tRNA^{Val} at a resolution of 3.0 Å (Fig. 5; Table S2 and Figs. S2 and S3b). This structure reveals that adding tRNA^{Val} to the A site stabilizes tRNA^{ProL} in the P/P configuration with the codon-anticodon in the +1 frame. There are, however, several differences between this structure and that of the ribosomal complex carrying a P/P-configured, unmodified Lys-tRNA^{ProL} in the +1 frame. While both

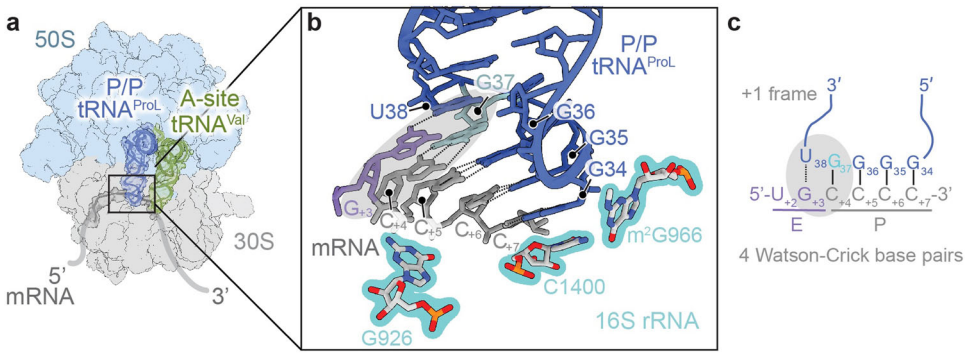

Fig. 5 | Accommodation of a tRNA into the A site stabilizes P site-bound, unmodified tRNA^{ProL} in the +1 frame. a A 3.0 Å cryo-EM structure of a POST– complex carrying an unmodified P-site tRNA^{ProL} paired to a CCC-C slippery codon in the +1 frame and an A-site, tRNA^{Val} bound to the GUU codon in the +1 frame. **b** Close-up of the codon-anticodon reveals four Watson-Crick base pairs and an interaction between U38 of the anticodon stem-loop and G$_{+3}$ of the codon. The additional base pairs are highlighted in gray (and in **c**). **c** A schematic of these interactions.

structures show that the tRNA^{ProL} interacts with the slippery codon in the +1 frame, there are only three Watson-Crick base pairs between the anticodon and the codon (G34-C$_{+7}$, G35-C$_{+6}$, and G36-C$_{+5}$) in the complex containing P/P-configured, unmodified Lys-tRNA^{ProL} (Fig. 4c). In the complex containing P/P-configured, unmodified tRNA^{ProL} and A/A-configured tRNA^{Val}, two new additional interactions occur: anticodon nucleotide G37 forms a Watson-Crick base pair with codon nucleotide C$_{+4}$ and codon nucleotide G$_{+3}$ moves towards the tRNA to form a single hydrogen bond with anticodon nucleotide U38 (Figs. 5b, c and S4b). This structure provides evidence that a four or five-base-pair codon-anticodon interaction can exist not only when the tRNA is translocating from the P to the E site, as we have captured here (Figs. 3 and 5), but also in the P site before the translocation event.

Discussion

In this study, we used an integrated structural biology approach to provide molecular insights into the importance of m^{1}G37 in the tRNA^{ProL} anticodon loop and how its absence leads to a +1 frameshift. Proline is a unique amino acid in that its cyclic side chain slows down peptidyl transfer rates on the ribosome, and its incorporation into the nascent polypeptide chain causes a distinct conformation in the exit tunnel[56,57]. These features of proline, which impact all three tRNA^{Pro} isoacceptors, do not explain why kinetic-, smFRET-, and structural studies show that +1 frameshifting occurs in distinct ways across the three tRNA^{Pro} isoacceptors[3,4,27,58]. Consistent with this, these mechanistic differences among the tRNA^{Pro} isoacceptors suggest that m^{1}G37 and the sequences of the tRNA and the codon all collectively influence the ability of these tRNA-mRNA pairs to undergo frameshifting[3,4,26,27,34,54,58]. Here, we focused on how the conformational energy of tRNA^{ProL} depends on the modification status of G37 and the slipperiness of the codon within the P site, the ribosomal tRNA binding site where this tRNA^{Pro} isoacceptor has been shown to undergo +1 frameshifting[3].

Using a bL9-uL1 smFRET signal, we characterized how POST− complexes fluctuate between GS1, in which the P site-bound tRNA^{ProL} is in the P/P configuration, and GS2, in which it is in the P/E configuration, as a function of the m^{1}G37 status of the tRNA and the slipperiness of the codon (Fig. 2). Our results show that when unmodified tRNA^{ProL} lacking the m^{1}G37 modification pairs with a slippery codon in the P site, the conformational energy of the tRNA is altered relative to that of native tRNA^{ProL} containing the m^{1}G37 modification. Specifically, when paired to a slippery codon, the conformational energy of native tRNA^{ProL} is such that this tRNA preferentially occupies the P/P configuration and exhibits a relatively high probability of fluctuating from P/E to the P/P configuration. In contrast, the conformational energy of unmodified tRNA^{ProL} is such that this tRNA preferentially occupies the P/E configuration and exhibits a relatively lower probability of fluctuating from the P/E configuration to the P/P configuration. This difference in the conformational energy of native *vs.* unmodified tRNA^{ProL} is not observed when both native and unmodified tRNA^{ProL} are paired to a non-slippery codon, demonstrating that the conformational energy of a P site-bound tRNA^{ProL} and, consequently, its ability to induce frameshifting depends not only on the modification status of G37, but also on the slipperiness of the codon. This finding strongly suggests that at a slippery codon, the disparate conformational energies of P site-bound native and unmodified tRNA^{ProL} allow these tRNAs to adopt different conformations at the P site. To arrive at this interpretation, it is important to note that the E^{FRET} value observed for GS2 in our bL9-uL1 smFRET signal cannot distinguish between an authentic GS2 state in which the tRNA adopts the P/E configuration and a 'GS2-like' state in which the tRNA adopts the e*/E configuration that has been previously observed in 70S POST− complexes carrying a P-site tRNA^{ProK}[27]. This ambiguity was a motivating factor for determining cryo-EM structures of such complexes.

Structures of the POST− complex in which the deacylated, unmodified tRNA^{ProL} is paired to a slippery codon show that this tRNA occupies the P/E configuration (Fig. 3), representative of the smFRET-observed GS2 state (Fig. 2). In this context, unmodified tRNA^{ProL} interacts with the slippery codon in the +1 frame (Figs. 3 and 6b). Most striking is the visualization of four Watson-Crick base pairs between

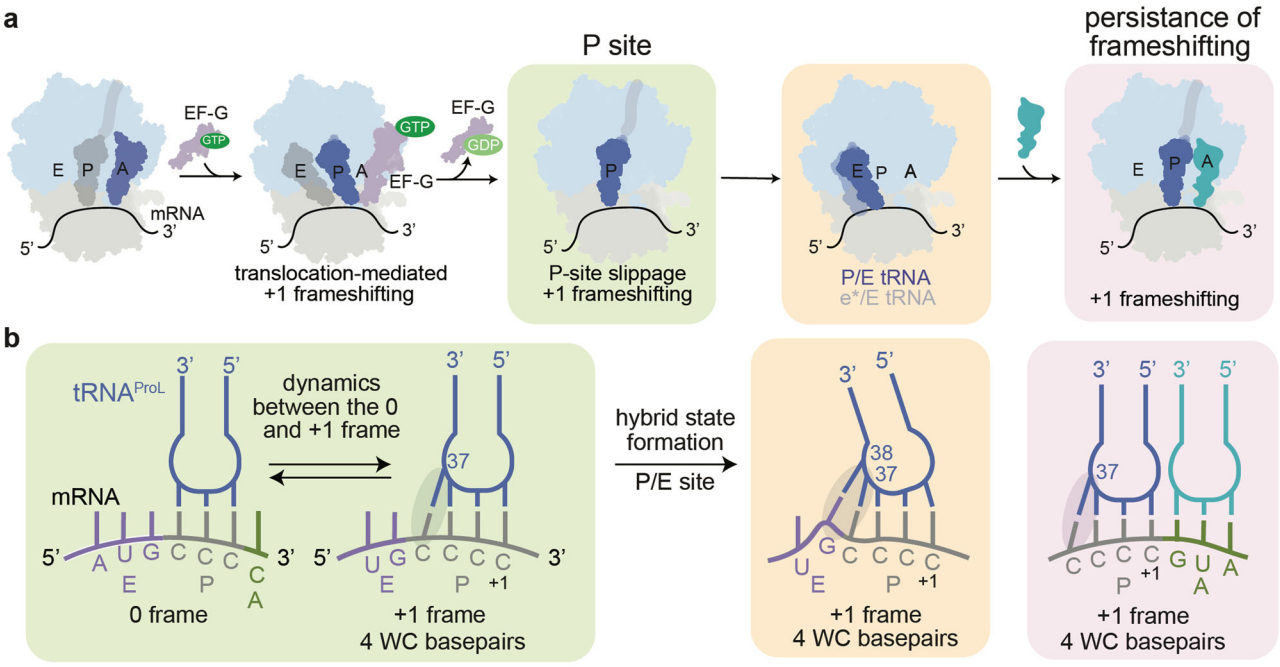

Fig. 6 | Mechanism by which m^{1}G37 influences the conformational energy of tRNA^{ProL} and modulates +1 frameshifting. a Unmodified peptidyl-tRNA^{ProL} can undergo +1 frameshifting either during the substep of the elongation cycle in which it is translocated from the A site into the P site (substeps in white background) or at the substep in which it has been translocated into the P site but has not yet undergone transfer of its peptidyl moiety onto the incoming aa-tRNA at the A site (complexes in light green and light orange background and substeps connecting them). Delivery of an aa-tRNA into the A site in the +1 frame stabilizes the P site-bound, +1 frameshifted, unmodified tRNA^{ProL} via stabilization of four Watson-Crick (WC) base pairs and an additional hydrogen bond at a fifth pairing (complex in light pink background). **b** Close-up view of WC base pairing and hydrogen bonding interactions formed within the various substeps and complexes in (**a**).

the anticodon and the codon with a fifth interaction forming between U38 of the anticodon stem-loop and codon nucleotide G_{+3} (Fig. 3). The propensity to form more than three Watson-Crick codon-anticodon base pairs on the ribosome has been predicted for decades[37,39,46,59–65] but had never been directly observed within a ribosomal complex. The four-nucleotide codon-anticodon model was mainly predicated on frameshift suppressor tRNA studies that undergo +1 frameshifts due to insertions in their anticodon loop, where this nucleotide insertion and the extra nucleotide of the suppressible codon form a Watson-Crick base pair. Only a single structure of a frameshift suppressor tRNA has been determined on the ribosome, and, while a movement into the +1 frame was observed, only three base pairs formed between the anticodon and the slippery codon, suggesting that the four-base-pair model could not explain the +1 frameshift[54]. Equally important are structures of other $tRNA^{Pro}$ isoacceptors that are either naturally frameshift prone ($tRNA^{ProM}$)[58] or which frameshift in the absence of the m^1G37 modification ($tRNA^{ProK}$[27] and $tRNA^{ProL}$ (this study)). Similar to the frameshift suppressor tRNA structure on the ribosome, although a +1 frameshift was observed, only three Watson-Crick base pairs form between the anticodon and the codon[27,58]. Our smFRET and structural studies of $tRNA^{ProL}$ demonstrate that it is possible to form four base pairs between the anticodon and the codon, but that the ability to do so is highly dependent upon the anticodon and codon sequences and can even vary among tRNA isoacceptors, e.g., $tRNA^{ProL}$, $tRNA^{ProM}$[58], and $tRNA^{ProK}$[27]. The remarkable mechanistic differences even among the different isoacceptors of the same tRNA underscore the difficulties in engineering tRNAs and/or mRNAs to recode the proteome using unnatural amino acid mutagenesis at four-base codons[66] or induce readthrough at premature stop codons[67].

Use of a nonhydrolyzable aminoacyl linkage allowed us to capture a POST complex containing Lys-$tRNA^{ProL}$ exclusively in the P/P configuration that supports $tRNA^{ProL}$ frameshifting[3] (Fig. 1b). The nonhydrolyzable aminoacyl linkage prevents deacylation of the Lys-$tRNA^{ProL}$ and restricts the 3′-end of the Lys-$tRNA^{ProL}$ to the 50S P site, preventing the Lys-$tRNA^{ProL}$ from stably occupying the P/E configuration and, consequently, the GS2 state (Fig. 4). Two distinct conformations of the codon-anticodon interaction were identified in structures of this POST complex, with one conformation showing the codon-anticodon interaction in the normal frame and the other conformation showing the codon-anticodon interaction in the +1 frame (Figs. 4 and 6b). In the +1 frame, a new fourth interaction between G37 of the anticodon stem-loop and the first nucleotide of the codon (C_{+4}) was revealed. Upon A-site tRNA binding, the codon-anticodon remains in the +1 frame, but now four Watson-Crick interactions and a fifth interaction consisting of a single hydrogen bond form between the anticodon and codon (Fig. 5). These data suggest that m^1G37 prevents an interaction with the first nucleotide of the codon (C_{+4}) to preserve the normal reading frame. Additionally, greater than three Watson-Crick interactions between the anticodon and codon are accommodated both in the P site and during its translocation from the P site to the E site (as in the P/E tRNA). Further, connecting the smFRET studies and the structures of the GS1 state, in the composition of the smFRET-observed GS1 state from the kinetic data, we hypothesize that in the context of a slippery sequence, the codon-anticodon subcomplex of the unmodified $tRNA^{ProL}$ likely adopts, and likely exchanges between, multiple conformations in the P site and that the preferential occupancy and/or exchange rates between these conformations is likely modulated by the absence/presence of an A-site tRNA.

The structures presented here provide evidence that four-nucleotide interactions between the anticodon and the codon can exist, but only when permitted by the specific architectural constraints imposed by the ribosome. In the case of tRNA-mediated +1 frameshifting, including that induced by $tRNA^{Pro}$ isoacceptors, frameshifting only occurs after peptidyl transfer and departure from the A site[3], corroborated by ribosome structures with P-site $tRNA^{ProK}$, P-site $tRNA^{ProM}$, and now P-site $tRNA^{ProL}$ paired to slippery codons[27,54,58,68] (Fig. 6a). These data suggest that the A site restricts four-nucleotide interactions between the anticodon and codon and, perhaps because of this, tRNA-mediated frameshifting in the A site is restricted and not typically observed.

Collectively, our findings allow us to propose a mechanistic model for the +1 frameshifting that is induced by $tRNA^{ProL}$ lacking the m^1 modification at nucleotide 37 (Fig. 6). In a POST complex, we hypothesize that the absence of m^1G37 destabilizes the anticodon stem-loop of P site-bound, unmodified peptidyl-$tRNA^{ProL}$, thereby altering its conformational energy and allowing it to form codon-anticodon interactions in either the normal or +1 frames. Interestingly, in the +1 frame, the codon-anticodon interaction consists of four Watson-Crick base pairs. This is the first time, to our knowledge, that an expanded codon-anticodon interaction has been observed to form. For the POST complexes in a +1 frame, delivery of the aa-tRNA encoded by the next codon in the +1 frame into the A site stabilizes the four Watson-Crick base pairing interactions that the P-site peptidyl-$tRNA^{ProL}$ anticodon makes with the slippery codon. After the peptidyl moiety of P-site peptidyl-$tRNA^{ProL}$ is transferred to the A-site aa-tRNA, the newly deacetylated $tRNA^{ProL}$ can adopt the P/E configuration, and it is in this configuration that its anticodon fully engages with the CCC-C slippery codon in the +1 frame. Within this geometry, four Watson-Crick base pairs form, with a fifth hydrogen bonding codon-anticodon interaction forming adjacent to the E site. Using smFRET and cryo-EM within an integrated structural biology approach has allowed us to elucidate the mechanism by which the m^1G modification suppresses +1 frameshifting and how, in its absence, the conformational energy of P-site $tRNA^{ProL}$ is altered to permit frameshifting. A particularly striking result, and feature of our model, is that the P site permits expanded interactions between the anticodon and codon that we hypothesize are maintained during further movements of deacylated $tRNA^{ProL}$ toward the E site.

Differences in the contributions that $tRNA^{Pro}$ isoacceptor modifications make to the conformational energetics of these ribosome-bound isoacceptors are likely responsible for the mechanistic distinctions that are observed across these isoacceptors (Fig. 6). For example, $tRNA^{ProM}$ inherently undergoes +1 frameshifting, regardless of its m^1G37 modification status, whereas $tRNA^{ProL}$ and $tRNA^{ProK}$ rely on the m^1 modification at G37 to suppress +1 frameshifting[3,35]. Additionally, while it is predicted that the role of m^1G37 in $tRNA^{ProL}$ and $tRNA^{ProK}$ is to suppress +1 frameshifts on slippery codons[8], other modifications, such as the cmo^5U34 modification in $tRNA^{ProM}$, may also influence frameshifting[35,36]. Consistent with this, $tRNA^{ProM}$ lacking all modifications, including cmo^5U34 and m^1G37, exhibits higher levels of frameshifting than $tRNA^{ProM}$ lacking only cmo^5U34[11]. Another important consideration is whether, in the +1 frame, the interaction between the anticodons of the different $tRNA^{Pro}$ isoacceptors and proline slippery codons is cognate in the +1 frame. Whereas the codon-anticodon interactions are cognate for both $tRNA^{ProM}$ and $tRNA^{ProL}$ on a CCC-C slippery codon, these interactions are near-cognate for $tRNA^{ProK}$ (there would be one mismatch within the codon-anticodon complex). The observation that these mechanistic differences are seen even within the same tRNA isoacceptor family emphasizes how differences in tRNA modification patterns, tRNA sequences, and mRNA codons and codon contexts can contribute to frame maintenance and faithful translation and protein synthesis. These insights will have implications in future studies that aim to engineer tRNAs for recoding experiments.

Methods

Purification of ribosomes, mRNA, and other translation components for smFRET experiments

A BL9-uL1 double deletion *E. coli* strain was used for purifying 30S and 50S subunits lacking ribosomal proteins BL9 and uL1 as previously described[42,43,69]. A variant of bL9 that carries a Gln-to-Cys substitution mutation at position 18 and a variant of uL1 that carries a Thr-to-Cys substitution mutation at position 202 were expressed, purified,

labeled with Cy3- and Cy5-maleimide (Lumiprobe Cat # 21380, 23380), respectively, and reconstituted into the 50S subunits lacking bL9 and uL1, following previously described protocols[43]. The in vitro transcribed mRNA containing the Shine-Dalgarno sequence, the AUG start codon, and the CCC-C slippery sequence, was hybridized to a 3′-biotinylated DNA oligonucleotide that was chemically synthesized by Integrated DNA Technologies (IDT)[69] (Table S5). Unmodified $tRNA^{ProL}$ was prepared by in vitro transcription. G37 of this tRNA was methylated by TrmD in the presence of AdoMet. Native *E. coli* $tRNA^{Val}$ and $tRNA^{ProL}$ were affinity purified, and *E. coli* $tRNA^{ProL}$ lacking the m^1 modification at G37 was purified from a strain in which TrmD expression was temperature sensitive[3]. All four tRNAs were charged by prolyl-tRNA synthetase (ProRS). $tRNA^{fMet}$ was aminoacylated and formylated by *E. coli* methionyl-tRNA synthetase and *E. coli* methionyl-tRNA formyltransferase[69] (MP Biomedicals Cat # MP219915410). Initiation Factor 1 (IF1), IF2, IF3, EF-Tu, EF-Ts, and EF-G were purified following previously published protocols[69].

POST− and POST complex formation for smFRET experiments

To prepare POST− complexes, we first assembled the 70S initiation complexes (ICs) and POST complexes in 50 mM Tris-OAc pH 7.0, 100 mM KCl, 5 mM NH_4OAc, 0.5 mM $Ca(OAc)_2$, 0.1 mM EDTA, 10 mM 2-mercaptoethanol, 5 mM putrescine dihydrochloride, and 1 mM spermidine (Tris-Polymix Buffer). Preparation of 70S ICs involved the following steps. First, 15 pmol of 30S, 27 pmol of IF1, 27 pmol of IF2, 27 pmol of IF3, 18 nmol of GTP, and 25 pmol of biotin-mRNA were incubated in 7 μL of Tris-Polymix Buffer at 5 mM $Mg(OAc)_2$ for 10 min at 37 °C. Then 20 pmol of fMet-$tRNA^{fMet}$ in 2 μL of 10 mM KOAc pH 5 and 10 pmol of bL9(Cy3)-labeled and uL1(Cy5)-labeled 50S subunits in 1 μL of Reconstitution Buffer (20 mM Tris-HCl pH 7.8, 8 mM $Mg(OAc)_2$, 150 mM NH_4Cl, 0.2 mM EDTA, and 5 mM 2-mercaptoethanol) were sequentially added to the mixture and the reaction was incubated for 10 min at 37 °C after each subsequent addition.

Separately, EF-Tu, GTP, and aa-$tRNA^{ProL}$ ternary complexes (TCs) were prepared as follows. First, 300 pmol of EF-Tu and 200 pmol of EF-Ts, supplemented with GTP Charging Components (1 mM GTP, 3 mM phosphoenolpyruvate, 2 units/mL pyruvate kinase), were incubated in 8 μL of Tris-Polymix Buffer with 5 mM $Mg(OAc)_2$ for 1 min at 37 °C. Next, the reaction was mixed with 30 pmol of aa-$tRNA^{ProL}$ in 2 μL of 25 mM NaOAc pH 5 and incubated for 1 min at 37 °C. The final 10 μL of TC was stored on ice until used for POST complex formation. A solution of GTP-bound EF-G was formed by incubating 120 pmol EF-G, supplemented with GTP Charging Components, in 5 μL of Tris-Polymix Buffer with 5 mM $Mg(OAc)_2$ for 2 min at room temperature. The POST complex was then assembled by incubating a mixture of 10 μL of the 70S IC, 10 μL of the TC, and 2.5 μL the GTP-bound EF-G solution for 5 min at room temperature. The POST complex reaction was adjusted to 100 μL with Tris-Polymix Buffer containing 20 mM $Mg(OAc)_2$, loaded onto a 10–40% (w/v) sucrose gradient prepared in Tris-Polymix Buffer with 20 mM $Mg(OAc)_2$, and purified via sucrose density gradient ultracentrifugation. Purified POST complexes were aliquoted, flash-frozen in liquid nitrogen, and stored at −80 °C.

POST− complexes were prepared immediately before use in smFRET experiments by incubating a mixture of 3 μL of POST complex, 2 μL of 10 mM puromycin solution, and 15 μL of Tris-Polymix Buffer containing 15 mM $Mg(OAc)_2$ for 10 min at room temperature.

smFRET experiments and data analysis

Ribosomal complexes were tethered to the streptavidin-derivatized, polyethylene glycol (PEG) (Laysan Bio Cat # mPEG-SVA-5000-1G) and biotinylated-PEG-passivated surface (Laysan Bio Cat # Biotin-PEG-SVA-5000-1G) of a quartz microfluidic flow cell via a biotin-streptavidin-biotin bridge. Imaging was performed in Tris-Polymix Buffer supplemented with 15 mM $Mg(OAc)_2$, an Oxygen-Scavenging System (2.5 mM protocatechuic acid pH 9 (Sigma-Aldrich Cat # 37580-25G-F) and 250 nM protocatechuate-3,4-dioxygenase pH 7.8 (Sigma-Aldrich Cat # P8279-25UN), and a Triplet-State-Quencher Cocktail (1 mM 1,3,5,7-cyclooctatetraene (Sigma-Aldrich Cat # 138924-1 G) and 1 mM 3-nitrobenzyl alcohol (Sigma-Aldrich Cat # 73148-5 G). POST− complexes were imaged at single-molecule resolution using a wide-field, prism-based total internal reflection fluorescence (TIRF) microscope. The Cy3 fluorophore was excited using a 532-nm, diode-pumped, solid-state laser (Laser Quantum) at a power of 18 mW, as measured at the prism, and the fluorescence emissions from both Cy3 and Cy5 were collected using a 1.2 numerical aperture, 60×, water-immersion objective (Nikon) and wavelength separated using a two-channel, simultaneous-imaging system (Dual View™, Optical Insights LLC). The Cy3 and Cy5 fluorescence emissions were imaged by recording a movie of the TIRF microscope field-of-view at an acquisition rate of 100 ms/frame using a 1024 × 1024 pixel, back-illuminated electron-multiplying charge-coupled-device (EMCCD) camera (Andor iXon Ultra 888) operating with 2 × 2 pixel binning controlled by software μManager 1.4. Each movie contained 600 frames because this 60-s time period was long enough to ensure that the majority of the Cy3 or Cy5 fluorophores in the field-of-view photobleached during the experiment, allowing for facile bleed-through and background corrections of the resulting trajectories (see below).

Image analysis for each movie was executed using the vbSCOPE custom Python code found in the Gonzalez Group's GitHub repository (https://github.com/GonzalezBiophysicsLab/ vbscope-paper)[70] and applying it as previously described[4,71]. Specifically, for each movie, fluorophore locations were identified, Cy3 and Cy5 imaging channels were aligned, and Cy3- and Cy5 fluorescence intensity *vs.* time trajectories were generated. The fluorescence intensity for Cy5 was corrected for Cy3 bleed-through by subtracting 5% of the fluorescence intensity for Cy3, and the Cy3 and Cy5 fluorescence intensities were baseline corrected using the EMCCD signal detected post-photobleaching. Only Cy3 and Cy5 fluorescence intensity *vs.* time trajectories in which the Cy3 and Cy5 fluorescence intensities were anti-correlated, as expected for FRET, and the Cy3 fluorescence intensity underwent a single-step Cy3 photobleaching event, as expected for imaging of an individual ribosomal complex, were used for further analyses. The E_{FRET} value at each time point for each trajectory was calculated using $E_{FRET} = I_{Cy5}/(I_{Cy5} + I_{Cy3})$, where I_{Cy3} and I_{Cy5} are baseline-corrected Cy3 and bleed-through-and baseline-corrected Cy5 fluorescence intensities. E_{FRET} values were then used to plot E_{FRET} vs. time trajectories corresponding to each pair of Cy3- and Cy5 fluorescence intensity *vs.* time trajectories.

The Viterbi paths, fractional populations of GS1 and GS2 (% GS1 and % GS2, respectively), the rates of transitions between GS1 and GS2 ($k_{GS1\to GS2}$ and $k_{GS2\to GS1}$), and the corresponding equilibrium constant (K_{eq}) (Supplementary Table S1), were then obtained using the vbFRET software program[72]. Specifically, we began by modeling the raw E_{FRET} *vs.* time trajectories using a Bayesian-estimated hidden Markov model (HMM). Information on the default vbFRET priors that were used for the Bayesian-based estimation is detailed in our previous work describing vbFRET[72]. Using the modeled data, the Viterbi algorithm could be used to determine the most probable path (*i.e.*, the Viterbi path) through GS1, GS2, and the photobleached state for each E_{FRET} *vs.* time trajectory. In addition, for each excursion to GS1, we extracted the dwell time spent in GS1 before transitioning to GS2, and for each excursion to GS2, we extracted the dwell time in GS2 before transitioning to GS1. % GS1 or % GS2 were then calculated by dividing the number of E_{FRET} data points in GS1 or GS2, respectively, by the total number of E_{FRET} data points and multiplying by 100. $k_{GS1\to GS2}$s and $k_{GS2\to GS1}$s were calculated by using the distribution of dwell times in GS1 or GS2 to build plots of the survival probability in GS1 or GS2, respectively. The average lifetimes in GS1 or GS2 ($t_{GS1,obs}$ or $t_{GS2,obs}$, respectively) were determined from the decay constants obtained from single exponential decay fits to the GS1 or GS2 survival

probability plots, respectively. $k_{GS1\rightarrow GS2}$ and $k_{GS2\rightarrow GS1}$ were determined using:

$$k_{GS1\rightarrow GS2} = \frac{1}{t_{GS1,obs}} - \frac{1}{t_{GS1,Photobleaching}} - \frac{1}{T} \quad (1)$$

$$k_{GS2\rightarrow GS1} = \frac{1}{t_{GS2,obs}} - \frac{1}{t_{GS2,Photobleaching}} - \frac{1}{T} \quad (2)$$

where $t_{Photobleaching}$, the lifetime of the E_{FRET} signal prior to photobleaching of either fluorophore, and T, the total observation time, are corrections for the premature truncation of E_{FRET} *vs.* time trajectories arising from either Cy3 or Cy5 photobleaching or by the finite length of our observation time, respectively[73]. Finally, K_{eq}s were calculated using the kinetic definition of the equilibrium constant, $K_{eq} = k_{GS1\rightarrow GS2}/k_{GS2\rightarrow GS1}$. As expected, the kinetically defined K_{eq}s are in very close agreement with the thermodynamically defined K_{eq}s ($K_{eq,thermo}$ = (% GS2)/(% GS1)).

Purification of ribosomes, mRNA, and tRNAs for structural studies

E. coli MRE600 70S ribosomes were purified as previously described[74]. mRNAs were chemically synthesized by IDT or in vitro transcribed and were designed to place an AUG in the E site; a proline CCC-C slippery codon in the P site, depending on the reading frame; and a GUU valine codon in the +1 reading frame in the A site (Table S5). Unmodified $tRNA^{ProL}$ transcripts were made by in vitro transcription[34]. Lys-$tRNA^{ProL}$ is a nonhydrolyzable aa-tRNA prepared by 3′-amino tailing of $tRNA^{ProL}$ transcript using CCA-adding enzyme, followed by flexizyme charging with lysine[47].

Cryo-EM complex formation, data collection, data processing, and modeling

Ribosome complexes were generated nonenzymatically by sequentially incubating *E. coli* 70S (0.5 μM), mRNA (1 μM), and 2.5 μM $tRNA^{ProL}$ (2.5 μM) (aminoacylated or deacylated) for 5 min each at 37 °C in ribosome buffer (10 mM HEPES-KOH pH 7.6, 10 mM $MgCl_2$, 100 mM NH_4Cl, and 6 mM β-mercaptoethanol) (Table S3, 4). For the unmodified $tRNA^{ProL}$ + $tRNA^{Val}$ dataset, 2.5 μM deacylated $tRNA^{Val}$ was incubated for an additional 5 min incubation[2]. Three μL of the complex was applied to glow-discharged C-flat Au 1.2/1.3 300 mesh grids (Electron Microscopy Science Cat # CF313-100-Au) at 100% humidity, blotted for 3 s before vitrification in liquid ethane by a Vitrobot Mark IV (Thermo Fisher Scientific), and stored in liquid nitrogen.

Both datasets were collected at the National Center for Cryo-EM Access and Training (NCCAT) using an FEI Krios 300 kV with the Gatan K3 imaging system with a 30 eV slit energy filter. The aa-$tRNA^{ProL}$ dataset was collected with the following parameters: 4467 micrographs of 50 frames, 1.069 Å pixel size, −0.6 to 2.5 μm defocus range, 56.07 $e^-/Å^2$ total dose rate, and 2.5 s exposure. The $tRNA^{ProL}$ + $tRNA^{Val}$ dataset was collected with the same setup and the following parameters: 10,949 micrographs, a −0.6 to 2.7 μm defocus range, and 61.23 $e^-/Å^2$ total dose rate.

All datasets were processed using RELION 3.0 and 3.1[75] (Figs. S2 and S7). Pre-processing was done using MotionCor2[76] and either CTFFIND4[77] or Gctf[78]. Ribosome particles were picked using template-free Laplacian-of-Gaussian autopicking followed by 2D classifications to discard non-ribosome particles. Ribosome classes with ligands bound were obtained from rounds of 3D classification using either a previous *E. coli* 70S or de novo initial model as a reference map, and masks around regions of interest (e.g., tRNA binding sites) for focused mask classifications. These classes were refined into 3D constructions, then post-processed in RELION[75] and autosharpened in Phenix[79]. Maps were examined in Coot, Chimera, and ChimeraX[80,81]. Local resolution maps were generated using ResMap[82] in RELION[75].

For modeling, 70S *E. coli* ribosome PDB code 6OM6 was used as the starting model for classes containing an unrotated 70S[83]. For the rotated 70S classes, PDB code 7SSW[84] was used for 70S classes containing e*/E-$tRNA^{ProL}$, and PDB code 6GXO[85] was used for 70S classes containing P/E-$tRNA^{ProL}$. Coordinates for $tRNA^{Val}$ and $tRNA^{ProK}$ are from PDB code 1VY4[86]. Models were docked into the cryo-EM maps in Chimera, then real-space refined in Phenix[87]. Final models were obtained from iterative rounds of model building in Coot and refinements in Phenix[80,87]. Figures were made in ChimeraX[81].

RADtool ribosome movement calculation

To determine the degree of 30S head swivel and tilting, the RADTool program was used[88]. The locations of 16S rRNA nucleotides 940, 984, and 1106 in the 30S body were compared because these nucleotides fluctuate less than 1 Å between different rotational states.

Reporting summary

Further information on research design is available in the Nature Portfolio Reporting Summary linked to this article.

Data availability

All of the analyzed smFRET data generated in this study are available in the Article and its Supplementary Information. The large, raw video files are available on request from the corresponding author (Gonzalez). The cryo-EM data generated in this study have been deposited in the PDB and Electron Microscopy Data Bank (EMSD) database under accession codes 8UTJ and EMD-42541 (https://doi.org/10.2210/pdb8UTJ/pdb); PDB code 8URM and EMD-42495 (https://doi.org/10.2210/pdb8URM/pdb); PDB code 8UXB and EMD-42721 (https://doi.org/10.2210/pdb8UXB/pdb); PDB code 8UX8 and EMD-42714 (https://doi.org/10.2210/pdb8UX8/pdb); PDB code 8V03 and EMD-42852 (https://doi.org/10.2210/pdb8V03/pdb); PDB code 8UZG and EMD-42840 (https://doi.org/10.2210/pdb8UZG/pdb).

References

1. Bjork, G. R., Wikstrom, P. M. & Bystrom, A. S. Prevention of translational frameshifting by the modified nucleoside 1-methylguanosine. *Science* **244**, 986–989 (1989).
2. Urbonavicius, J., Qian, Q., Durand, J. M., Hagervall, T. G. & Bjork, G. R. Improvement of reading frame maintenance is a common function for several tRNA modifications. *EMBO J.* **20**, 4863–4873 (2001).
3. Gamper, H. B., Masuda, I., Frenkel-Morgenstern, M. & Hou, Y. M. Maintenance of protein synthesis reading frame by EF-P and m(1) G37-tRNA. *Nat. Commun.* **6**, 7226 (2015).
4. Gamper, H. et al. Insights into genome recoding from the mechanism of a classic +1-frameshifting tRNA. *Nat. Commun.* **12**, 328 (2021).
5. Atkins, J. F., Gesteland, R. F., Reid, B. R. & Anderson, C. W. Normal tRNAs promote ribosomal frameshifting. *Cell* **18**, 1119–1131 (1979).
6. Smith, A. M., Costello, M. S., Kettring, A. H., Wingo, R. J. & Moore, S. D. Ribosome collisions alter frameshifting at translational reprogramming motifs in bacterial mRNAs. *Proc. Natl. Acad. Sci. USA* **116**, 21769–21779 (2019).
7. Masuda, I. et al. tRNA methylation resolves codon usage bias at the limit of cell viability. *Cell Rep.* **41**, 111539 (2022).
8. Hou, Y. M., Masuda, I. & Gamper, H. Codon-Specific Translation by m(1)G37 Methylation of tRNA. *Front Genet.* **9**, 713 (2018).
9. Farabaugh, P. J. Programmed translational frameshifting. *Annu. Rev. Genet.* **30**, 507–528 (1996).
10. Dinman, J. D. Control of gene expression by translational recoding. *Adv. Protein Chem. Struct. Biol.* **86**, 129–149 (2012).
11. Dunkle, J. A. & Dunham, C. M. Mechanisms of mRNA frame maintenance and its subversion during translation of the genetic code. *Biochimie* **114**, 90–96 (2015).
12. Craigen, W. J., Cook, R. G., Tate, W. P. & Caskey, C. T. Bacterial peptide chain release factors: conserved primary structure and possible frameshift regulation of release factor 2. *Proc. Natl. Acad. Sci. USA* **82**, 3616–3620 (1985).

13. Baranov, P. V., Gesteland, R. F. & Atkins, J. F. Release factor 2 frameshifting sites in different bacteria. *EMBO Rep.* **3**, 373–377 (2002).
14. Gao, W., Jakubowski, H. & Goldman, E. Evidence that uncharged tRNA can inhibit a programmed translational frameshift in Escherichia coli. *J. Mol. Biol.* **251**, 210–216 (1995).
15. van Weringh, A. et al. HIV-1 modulates the tRNA pool to improve translation efficiency. *Mol. Biol. Evol.* **28**, 1827–1834 (2011).
16. Girstmair, H. et al. Depletion of cognate charged transfer RNA causes translational frameshifting within the expanded CAG stretch in huntingtin. *Cell Rep.* **3**, 148–159 (2013).
17. Atkins, J. F. Loughran, G. Bhatt, P. R. Firth, A. E. Baranov, P. V. Ribosomal frameshifting and transcriptional slippage: from genetic steganography and cryptography to adventitious use. *Nucleic Acids Res.* **44**, 7007–7078 (2016).
18. Caliskan, N. et al. Conditional Switch between Frameshifting Regimes upon Translation of dnaX mRNA. *Mol. Cell* **66**, 558–567.e554 (2017).
19. Korniy, N. et al. Modulation of HIV-1 Gag/Gag-Pol frameshifting by tRNA abundance. *Nucleic Acids Res.* **47**, 5210–5222 (2019).
20. Agris, P. F. et al. Celebrating wobble decoding: half a century and still much is new. *RNA Biol.* **15**, 537–553 (2018).
21. de Crecy-Lagard, V. & Jaroch, M. Functions of bacterial tRNA modifications: from ubiquity to diversity. *Trends Microbiol.* **29**, 41–53 (2021).
22. Boccaletto, P. et al. MODOMICS: a database of RNA modification pathways. 2017 update. *Nucleic Acids Res.* **46**, D303–D307 (2018).
23. Sundaram, M., Durant, P. C. & Davis, D. R. Hypermodified nucleosides in the anticodon of tRNA(Lys) stabilize a canonical U-turn structure. *Biochemistry* **39**, 15652 (2000).
24. Murphy, F. V. T., Ramakrishnan, V., Malkiewicz, A. & Agris, P. F. The role of modifications in codon discrimination by tRNA(Lys)UUU. *Nat. Struct. Mol. Biol.* **11**, 1186–1191 (2004).
25. Machnicka, M. A., Olchowik, A., Grosjean, H. & Bujnicki, J. M. Distribution and frequencies of post-transcriptional modifications in tRNAs. *RNA Biol.* **11**, 1619–1629 (2014).
26. Nguyen, H. A., Hoffer, E. D. & Dunham, C. M. Importance of a tRNA anticodon loop modification and a conserved, noncanonical anticodon stem pairing in tRNACGGProfor decoding. *J. Biol. Chem.* **294**, 5281–5291 (2019).
27. Hoffer E. D. et al. Structural insights into mRNA reading frame regulation by tRNA modification and slippery codon-anticodon pairing. *Elife* **9**, e51898 (2020).
28. Bystrom, A. S. & Bjork, G. R. Chromosomal location and cloning of the gene (trmD) responsible for the synthesis of tRNA (m1G) methyltransferase in Escherichia coli K-12. *Mol. Gen. Genet.* **188**, 440–446 (1982).
29. Subramanian, M., Srinivasan, T. & Sudarsanam, D. Examining the Gm18 and m(1)G Modification Positions in tRNA Sequences. *Genomics Inf.* **12**, 71–75 (2014).
30. Hagervall, T. G., Tuohy, T. M., Atkins, J. F. & Bjork, G. R. Deficiency of 1-methylguanosine in tRNA from Salmonella typhimurium induces frameshifting by quadruplet translocation. *J. Mol. Biol.* **232**, 756–765 (1993).
31. Clifton, B. E., Fariz, M. A., Uechi, G. I. & Laurino, P. Evolutionary repair reveals an unexpected role of the tRNA modification m1G37 in aminoacylation. *Nucleic Acids Res.* **49**, 12467–12485 (2021).
32. Masuda, I. et al. Loss of N(1)-methylation of G37 in tRNA induces ribosome stalling and reprograms gene expression. *Elife* **10**, e70619 (2021).
33. O'Connor, M. Imbalance of tRNA(Pro) isoacceptors induces +1 frameshifting at near-cognate codons. *Nucleic Acids Res.* **30**, 759–765 (2002).
34. Gamper, H. et al. Twice exploration of tRNA +1 frameshifting in an elongation cycle of protein synthesis. *Nucleic Acids Res.* **49**, 10046–10060 (2021).
35. Gamper, H. B., Masuda, I., Frenkel-Morgenstern, M. & Hou, Y. M. The UGG isoacceptor of tRNAPro is naturally prone to frameshifts. *Int J. Mol. Sci.* **16**, 14866–14883 (2015).
36. Masuda, I. et al. Selective terminal methylation of a tRNA wobble base. *Nucleic Acids Res.* **46**, e37 (2018).
37. Yourno, J. Externally suppressible +1 "glycine" frameshift: possible quadruplet isomers for glycine and proline. *Nat. N. Biol.* **239**, 219–221 (1972).
38. Riddle, D. L. & Carbon, J. Frameshift suppression: a nucleotide addition in the anticodon of a glycine transfer RNA. *Nat. N. Biol.* **242**, 230–234 (1973).
39. Curran, J. F. & Yarus, M. Reading frame selection and transfer RNA anticodon loop stacking. *Science* **238**, 1545–1550 (1987).
40. Magliery, T. J., Anderson, J. C. & Schultz, P. G. Expanding the genetic code: selection of efficient suppressors of four-base codons and identification of "shifty" four-base codons with a library approach in Escherichia coli. *J. Mol. Biol.* **307**, 755–769 (2001).
41. Fei, J., Richard, A. C., Bronson, J. E. & Gonzalez, R. L. Jr. Transfer RNA-mediated regulation of ribosome dynamics during protein synthesis. *Nat. Struct. Mol. Biol.* **18**, 1043–1051 (2011).
42. Fei, J., Kosuri, P., MacDougall, D. D. & Gonzalez, R. L. Jr. Coupling of ribosomal L1 stalk and tRNA dynamics during translation elongation. *Mol. Cell* **30**, 348–359 (2008).
43. Fei, J. et al. Allosteric collaboration between elongation factor G and the ribosomal L1 stalk directs tRNA movements during translation. *Proc. Natl. Acad. Sci. USA* **106**, 15702–15707 (2009).
44. Ban, N. et al. A new system for naming ribosomal proteins. *Curr. Opin. Struct. Biol.* **24**, 165–169 (2014).
45. Zhang, W., Dunkle, J. A. & Cate, J. H. Structures of the ribosome in intermediate states of ratcheting. *Science* **325**, 1014–1017 (2009).
46. Riddle, D. L. & Roth, J. R. Frameshift suppressors. 3. Effects of suppressor mutations on transfer RNA. *J. Mol. Biol.* **66**, 495–506 (1972).
47. Murakami, H., Ohta, A., Ashigai, H. & Suga, H. A highly flexible tRNA acylation method for non-natural polypeptide synthesis. *Nat. Methods* **3**, 357–359 (2006).
48. Gamper, H. & Hou, Y. M. tRNA 3'-amino-tailing for stable amino acid attachment. *RNA* **24**, 1878–1885 (2018).
49. Selmer, M. et al. Structure of the 70S ribosome complexed with mRNA and tRNA. *Science* **313**, 1935–1942 (2006).
50. Rheinberger, H. J., Sternbach, H. & Nierhaus, K. H. Three tRNA binding sites on Escherichia coli ribosomes. *Proc. Natl. Acad. Sci. USA* **78**, 5310–5314 (1981).
51. Lill, R., Robertson, J. M. & Wintermeyer, W. Affinities of tRNA binding sites of ribosomes from Escherichia coli. *Biochemistry* **25**, 3245–3255 (1986).
52. Zhou, J., Lancaster, L., Donohue, J. P. & Noller, H. F. Crystal structures of EF-G-ribosome complexes trapped in intermediate states of translocation. *Science* **340**, 1236086 (2013).
53. Zhou, J., Lancaster, L., Donohue, J. P. & Noller, H. F. How the ribosome hands the A-site tRNA to the P site during EF-G-catalyzed translocation. *Science* **345**, 1188–1191 (2014).
54. Hong, S. et al. Mechanism of tRNA-mediated +1 ribosomal frameshifting. *Proc. Natl. Acad. Sci. USA* **115**, 11226–11231 (2018).
55. Zhou, J., Lancaster, L., Donohue, J. P. & Noller, H. F. Spontaneous ribosomal translocation of mRNA and tRNAs into a chimeric hybrid state. *Proc. Natl. Acad. Sci. USA* **116**, 7813–7818 (2019).
56. Pierson, W. E. et al. Uniformity of peptide release is maintained by methylation of release factors. *Cell Rep.* **17**, 11–18 (2016).
57. Huter, P. et al. Structural basis for polyproline-mediated ribosome stalling and rescue by the translation elongation factor EF-P. *Mol. Cell* **68**, 515–527.e516 (2017).
58. Demo, G. et al. Structural basis for +1 ribosomal frameshifting during EF-G-catalyzed translocation. *Nat. Commun.* **12**, 4644 (2021).

59. Riyasaty, S. & Atkins, J. F. External suppression of a frameshift mutant in Salmonella. *J. Mol. Biol.* **34**, 541–557 (1968).
60. Prather, N. E., Murgola, E. J. & Mims, B. H. Nucleotide insertion in the anticodon loop of a glycine transfer RNA causes missense suppression. *Proc. Natl. Acad. Sci. USA* **78**, 7408–7411 (1981).
61. Cummins, C. M., Donahue, T. F. & Culbertson, M. R. Nucleotide sequence of the SUF2 frameshift suppressor gene of Saccharomyces cerevisiae. *Proc. Natl. Acad. Sci. USA* **79**, 3565–3569 (1982).
62. Yarus, M. Translational efficiency of transfer RNA's: uses of an extended anticodon. *Science* **218**, 646–652 (1982).
63. Gaber, R. F. & Culbertson, M. R. Codon recognition during frameshift suppression in Saccharomyces cerevisiae. *Mol. Cell Biol.* **4**, 2052–2061 (1984).
64. Moore, B., Persson, B. C., Nelson, C. C., Gesteland, R. F. & Atkins, J. F. Quadruplet codons: implications for code expansion and the specification of translation step size. *J. Mol. Biol.* **298**, 195–209 (2000).
65. Anderson, J. C., Magliery, T. J. & Schultz, P. G. Exploring the limits of codon and anticodon size. *Chem. Biol.* **9**, 237–244 (2002).
66. Siddika, T. Heinemann, I. U. Donoghue, P. O'. Expanding codon size. *Elife* **11**, e78869 (2022).
67. Albers, S. et al. Engineered tRNAs suppress nonsense mutations in cells and in vivo. *Nature* **618**, 842–848 (2023).
68. Maehigashi, T., Ruangprasert, A., Miles, S. J. & Dunham, C. M. Molecular basis of ribosome recognition and mRNA hydrolysis by the E. coli YafQ toxin. *Nucleic Acids Res.* **43**, 8002–8012 (2015).
69. Fei, J. et al. A highly purified, fluorescently labeled in vitro translation system for single-molecule studies of protein synthesis. *Methods Enzymol.* **472**, 221–259 (2010).
70. Verma, A. R. Ray, K. K. Bodick, M. Kinz-Thompson, C. D. Gonzalez, Jr., R. L. Increasing the accuracy of single-molecule data analysis using tMAVEN. *Biophys J*. https://doi.org/10.1101/2023.08.15.553409 (2024).
71. Ray, K. K. et al. Entropic control of the free-energy landscape of an archetypal biomolecular machine. *Proc. Natl. Acad. Sci. USA* **120**, e2220591120 (2023).
72. Bronson, J. E., Fei, J., Hofman, J. M., Gonzalez, R. L. Jr. & Wiggins, C. H. Learning rates and states from biophysical time series: a Bayesian approach to model selection and single-molecule FRET data. *Biophys. J.* **97**, 3196–3205 (2009).
73. Sternberg, S. H., Fei, J., Prywes, N., McGrath, K. A. & Gonzalez, R. L. Jr. Translation factors direct intrinsic ribosome dynamics during translation termination and ribosome recycling. *Nat. Struct. Mol. Biol.* **16**, 861–868 (2009).
74. Zhang, Y., Hong, S., Ruangprasert, A., Skiniotis, G. & Dunham, C. M. Alternative mode of E-Site tRNA binding in the presence of a downstream mRNA stem loop at the entrance channel. *Structure* **26**, 437–445.e433 (2018).
75. Zivanov, J. et al. New tools for automated high-resolution cryo-EM structure determination in RELION-3. *Elife* **7**, e42166 (2018).
76. Zheng, S. Q. et al. MotionCor2: anisotropic correction of beam-induced motion for improved cryo-electron microscopy. *Nat. Methods* **14**, 331–332 (2017).
77. Rohou, A. & Grigorieff, N. CTFFIND4: fast and accurate defocus estimation from electron micrographs. *J. Struct. Biol.* **192**, 216–221 (2015).
78. Zhang, K. Gctf: real-time CTF determination and correction. *J. Struct. Biol.* **193**, 1–12 (2016).
79. Terwilliger, T. C., Sobolev, O. V., Afonine, P. V. & Adams, P. D. Automated map sharpening by maximization of detail and connectivity. *Acta Crystallogr. D. Struct. Biol.* **74**, 545–559 (2018).
80. Emsley, P., Lohkamp, B., Scott, W. G. & Cowtan, K. Features and development of Coot. *Acta Crystallogr D. Biol. Crystallogr* **66**, 486–501 (2010).
81. Pettersen, E. F. et al. UCSF ChimeraX: structure visualization for researchers, educators, and developers. *Protein Sci.* **30**, 70–82 (2021).
82. Kucukelbir, A., Sigworth, F. J. & Tagare, H. D. Quantifying the local resolution of cryo-EM density maps. *Nat. Methods* **11**, 63–65 (2014).
83. Aron, Z. D. et al. trans-Translation inhibitors bind to a novel site on the ribosome and clear Neisseria gonorrhoeae in vivo. *Nat. Commun.* **12**, 1799 (2021).
84. Carbone, C. E. et al. Time-resolved cryo-EM visualizes ribosomal translocation with EF-G and GTP. *Nat. Commun.* **12**, 7236 (2021).
85. Graf, M. et al. Visualization of translation termination intermediates trapped by the Apidaecin 137 peptide during RF3-mediated recycling of RF1. *Nat. Commun.* **9**, 3053 (2018).
86. Polikanov, Y. S., Steitz, T. A. & Innis, C. A. A proton wire to couple aminoacyl-tRNA accommodation and peptide-bond formation on the ribosome. *Nat. Struct. Mol. Biol.* **21**, 787–793 (2014).
87. Liebschner, D. et al. Macromolecular structure determination using X-rays, neutrons and electrons: recent developments in Phenix. *Acta Crystallogr. D. Struct. Biol.* **75**, 861–877 (2019).
88. Hassan, A. et al. Ratchet, swivel, tilt and roll: a complete description of subunit rotation in the ribosome. *Nucleic Acids Res.* **51**, 919–934 (2023).

Acknowledgements

This work was supported by the NIH R01 GM093278 and R35 GM156629 (to C.M.D.), R01 GM119386 and R35 GM153724 (to R.L.G., Jr.), and R35 GM134931 (to Y-M.H.)) and by the NSF (CHE 1808711 to C.M.D.). HL was supported by a Charles H. Revson Foundation Postdoctoral Fellowship in Biomedical Science 19-24. Initial screening was performed at the Emory University Robert P. Apkarian Integrated Electron Microscopy Core, under the supervision of Dr. Ricardo Guerrero-Ferreira. Cryo-EM datasets were collected at the National Center for Cryo-EM Access and Training (NCCAT) and the Simons Electron Microscopy Center located at the New York Structural Biology Center. These centers are supported by the NIH Common Fund Transformative High Resolution Cryo-Electron Microscopy program (U24 GM129539) and by grants from the Simons Foundation (SF349247) and NY State Assembly. We thank Dunham lab members Pooja Srinivas and Tiffany Trieu for providing comments on the manuscript.

Author contributions

All authors (E.M.K., H.A.N., H.L., J.M.M., N.A.B., W.N., H.G., Y-M.H., R.L.G.,Jr. and C.M.D.) contributed to the designed research; E.M.K., H.A.N., H.L., J.M.M., N.A.B., W.N. and H.G. performed the research; and E.M.K., H.A.N., H.L., N.A.B. and W.N. analyzed the data; and all authors (E.M.K., H.A.N., H.L., J.M.M., N.A.B., W.N., H.G., Y-M.H., R.L.G.,Jr. and C.M.D.) contributed to the writing of the paper.

Competing interests

The authors declare no competing interests.

Additional information

Supplementary information The online version contains supplementary material available at https://doi.org/10.1038/s41467-025-62342-4.

Correspondence and requests for materials should be addressed to Ruben L. Gonzalez or Christine M. Dunham.

Peer review information *Nature Communications* thanks the anonymous reviewers for their contribution to the peer review of this work. A peer review file is available.

Reprints and permissions information is available at http://www.nature.com/reprints

Publisher's note Springer Nature remains neutral with regard to jurisdictional claims in published maps and institutional affiliations.

Open Access This article is licensed under a Creative Commons Attribution-NonCommercial-NoDerivatives 4.0 International License, which permits any non-commercial use, sharing, distribution and reproduction in any medium or format, as long as you give appropriate credit to the original author(s) and the source, provide a link to the Creative Commons licence, and indicate if you modified the licensed material. You do not have permission under this licence to share adapted material derived from this article or parts of it. The images or other third party material in this article are included in the article's Creative Commons licence, unless indicated otherwise in a credit line to the material. If material is not included in the article's Creative Commons licence and your intended use is not permitted by statutory regulation or exceeds the permitted use, you will need to obtain permission directly from the copyright holder. To view a copy of this licence, visit http://creativecommons.org/licenses/by-nc-nd/4.0/.

© The Author(s) 2025